applied optics

Design and fabrication of copper-filled photonic crystal fiber based polarization filters

Mohd Fahmi Azman,[1,*] Ghafour Amouzad Mahdiraji,[2,4,5] Wei Ru Wong,[1] Rifat Ahmmed Aoni,[3] and Faisal Rafiq Mahamd Adikan[1,4,6]

[1]Integrated Lightwave Research Group, Electrical Department, Faculty of Engineering, Universiti Malaya, 50603 Lembah Pantai, Kuala Lumpur, Malaysia
[2]School of Engineering, Faculty of Technology and Innovation, Taylor's University, 47500 Subang Jaya, Selangor, Malaysia
[3]Nonlinear Physics Centre, Research School of Physics and Engineering, The Australian National University, Canberra Acton 2601, Australia
[4]Flexilicate Sdn. Bhd., Faculty of Engineering, University Malaya, 50603 Lembah Pantai, Kuala Lumpur, Malaysia
[5]e-mail: ghafouram@gmail.com
[6]e-mail: rafiq@um.edu.my
*Corresponding author: fahmibinazman@gmail.com

Received 3 January 2019; revised 20 February 2019; accepted 20 February 2019; posted 20 February 2019 (Doc. ID 356641); published 8 March 2019

This work demonstrates a broadband polarization filter based on copper-filled photonic crystal fiber (CFPCF). The proposed fiber is fabricated using the conventional stack-and-draw method. The polarization filter properties of the proposed CFPCF are investigated numerically by considering the cross-sectional scanning electron microscopy image of the fabricated CFPCF. It is observed that the magnitude of cross talk reached up to −206 dB over 0.8 mm length with a broad bandwidth of 282 nm at a central wavelength of 1790 nm. In addition, the polarization characteristics of the CFPCF including cross talk, central wavelength, and bandwidth can be adjusted by varying the diameter of the copper wire. It is shown that the resonance wavelength of the proposed filter can be tuned over the wide range of wavelengths from 1390 to 1890 nm. We have shown that by adjusting the copper wire diameter to 0.32Λ and 0.48Λ μm (Λ is pitch size), the proposed filter can operate at communication bands of 1310 and 1550 nm, respectively. The results suggest high-potential of the proposed fiber for polarization filtering and other sensing applications.

https://doi.org/10.1364/AO.58.002068

1. INTRODUCTION

The fabrication of miniaturized and integrated in-fiber devices of an optical system has driven a lot of research interest [1–5]. Since the birth of photonic crystal fibers (PCFs) in 1995, PCF has been extensively practiced in many fields, such as biosensors [6], passive optical devices [7,8], and medicine [3], owing to its structural flexibility [9–12]. Recently, the incorporation of different materials, such as liquid crystals [13], polymer [14], and semiconductors [10], into the selective hollow channel in a PCF has been demonstrated to modify its optical interaction. Consequently, a strong polarized-wavelength-dependent transmission (PWDT) has been discovered by incorporating selectively a metal wire into the air-hole channel of the PCFs [15]. The PWDT property is caused by the surface plasmon polariton (SPP), which is excited at the metal–dielectric interface due to the stimulation of light. Consequently, this phenomenon has already been studied in many potential applications including polarizers [16–20], sensors [4,6,21], and in-fiber devices [2,5,22].

At the resonance wavelength, the fiber core-guided mode in a PCF will eventually couple to the evanescent field of the SPP mode when their phases match. To date, several attempts have been made to fabricate a metal incorporated PCF, by coating or filling selectively the air hole with metal for the excitation of SPP. In 1993, Jorgenson *et al.* demonstrated a technique to coat the core of a multimode fiber with a metal layer [23]. The fabrication process began by removing the cladding of the optical fiber to expose the core and a thin film of metal layer was deposited onto the core. On the other hand, in 2007, Zhang *et al.* reported a selective silver (Ag) coating into the hollow channel of PCFs [24]. Unlike previous methods, Tyagi *et al.* reported in 2010 a fabrication technique for gold (Au) nanowires which were placed next to the core of a step-index fiber [25]. They used Au in a glass capillary and drew the structure into smaller dimensions up to 260 nm by applying direct drawing. The authors also developed a method to incorporate the Au wire in a PCF by vacuuming the molten Au at a very high pressure into the hollow channels [26]. The authors observed the PWDT characteristic from the SPP resonance of the Au nanowire and the fiber core. There are a number of numerical studies on the polarization characteristics of

metal-filled PCF that have been reported recently [8,15–21,24,27–29]. On the other hand, Xue *et al.* in 2013 reported a polarization filter of Au-coated PCF and claimed that the resonance loss at 1311 nm wavelength was 508 dB/cm in *y*-polarization. However, the full width half-maximum (FWHM) achieved was 20 nm [16]. In 2015, Heikal *et al.* observed the resonance loss of the polarization filter with *x*-polarization as 774.04 dB/cm at 1013 nm wavelength for an Au-filled spiral structure of PCF. Also, they quoted that the coupling of the SPP mode to the core-guided mode is tunable by adding more metal rod into the hollow channel [19]. The most recent literature presented a PCF of symmetrical structure with the presence of small air holes near the fiber core region [29]. The paper reported that *y*-polarized direction could filter the wavelength from 1200 to 1700 nm with a resonance loss of 214.23 dB/cm at the wavelength of 1310 nm. To the best of our knowledge, there are no reports demonstrating practical fabrication of a polarization filter based on PCFs.

Apart from noble metals (Au and Ag), copper (Cu) also possesses good optical properties. The permittivity and refractive index value for Au and Cu are almost identical compared to Ag from the wavelength range of 200 to 1900 nm [30,31]. Moreover, despite widespread availability, Cu is relatively cheaper compared to Au and Ag. For the proposed polarization filter fabrication process, which follows the stack-and-draw method (top-down approach) and requires larger size of raw material, Cu is the most suitable metal to generate mass production and it is obtainable at a very low cost compared to Au and Ag. Experimentally, Cu is compatible with glass and there is no reaction between both materials during the fabrication process and have been reported in [15]. This paper presents numerical and experimental analyses of a copper-filled photonic crystal fiber (CFPCF) proposed as a polarization filter. The filtering characteristics of the proposed PCF, including the resonance loss, cross talk, insertion loss, and optical bandwidth, are studied extensively. By adjusting the diameter of the metal, the loss peak of *x*- and *y*-polarized modes can be tuned, and hence the filtering range can be changed from 1390 to 1890 nm. The findings in this paper will contribute significantly to the field of passive optical and fiber-based plasmonic devices.

2. STRUCTURAL DESIGN AND FABRICATION OF CFPCF

Figure 1 exhibits the conceptual model of the structural design of the proposed CFPCF-based polarization filter. The center of the CFPCF is a silica rod as the fiber's core with the diameter of $d_{\text{core}} = 8$ μm. In order to reduce the leaky modes and propagation loss, the proposed CFPCF consists of six rings of air holes with air-channels diameter of $d_a = 4.71$ μm. The air-channels diameter was calculated proportionally with the ratio of the outer diameter (OD) and inner diameter of the available silica tube. The distance between the adjacent air holes known as the pitch is determined as $\Lambda = 6.73$ μm. Cu has been used in the proposed CFPCF because of its cost-effectiveness and its plasmonic behavior is as close to gold. The diameter of the copper wire d_c was varied to study the impact of d_c on the polarization properties of the CFPCF.

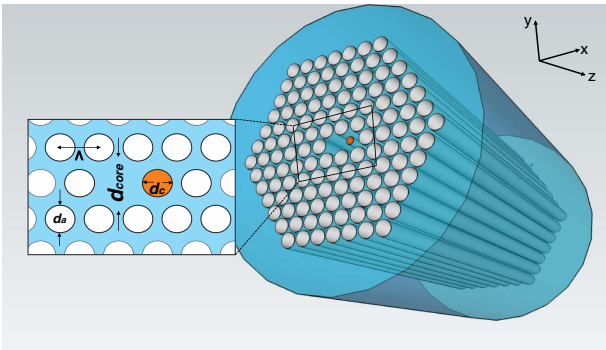

Fig. 1. 3D sketch and cross section of the conceptual design of a CFPCF-based polarization filter.

The CFPCF-based polarization filter was fabricated by using the stack-and-draw method as described previously in [32]. As graphically illustrated in Fig. 2, the CFPCF was developed by preparing a silica rod of 1.34 mm as the fiber core, 126 capillaries with an OD of 1.34, and a 1.0 mm diameter copper rod placed inside one of the capillaries. One head of all capillaries was sealed except that which contains the copper rod. The stacking process was performed in a hexagonal jig and then transferred into a perform tube. The perform was then drawn into cane size (~2 mm in OD) while a vacuum pressure was applied from the top of the perform to collapse the interstitial holes as well as fitting the copper wire inside the capillary. Later,

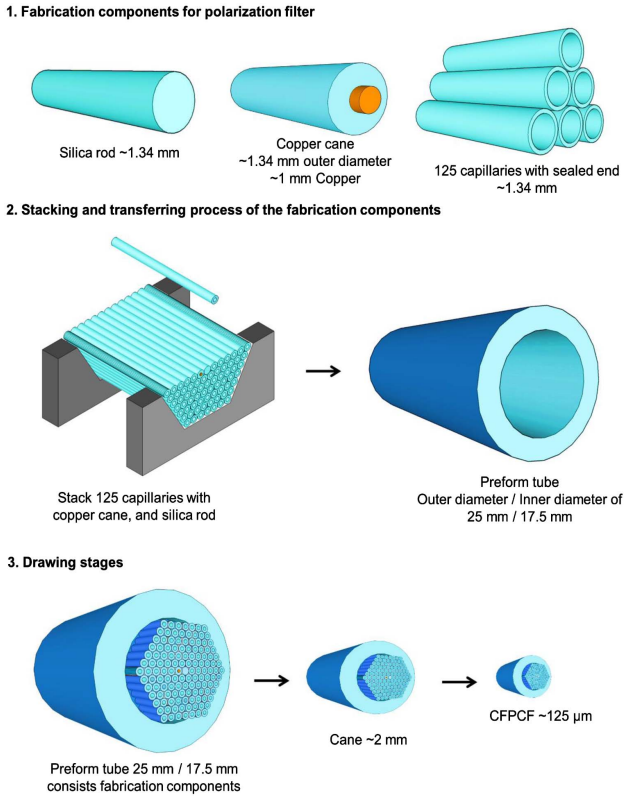

Fig. 2. Illustration for summarizing the fabrication process of CFPCF.

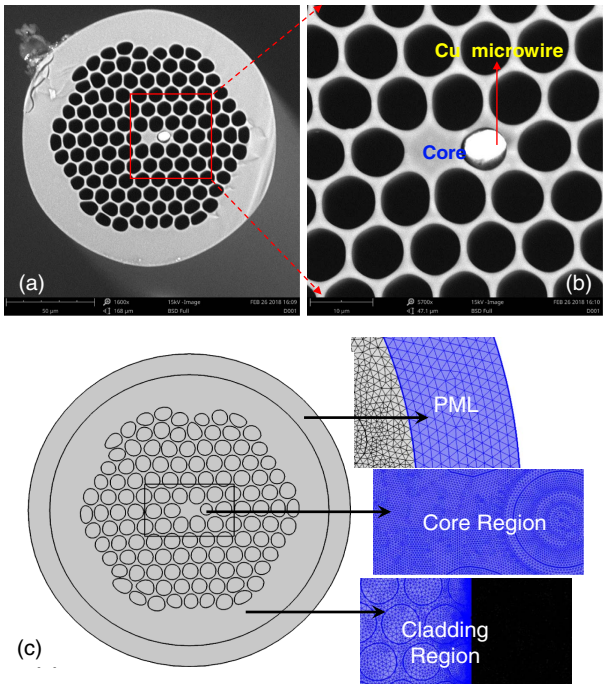

Fig. 3. (a) SEM image of the cross-sectional structure of CFPCF. (b) Magnified view of the core area of CFPCF indicating the presence of copper and a solid core. (c) The extracted SEM image from COMSOL with meshing structure for PML, core, and cladding region.

a CFPCF cane was re-drawn into the desired fiber size (125 μm in OD).

Figure 3 shows the scanning electron microscopy (SEM) image of the fabricated CFPCF. The SEM image of the fabricated CFPCF was used for all simulation studies reported in this paper. The simulation study was carried out by using COMSOL Multiphysics 5.3 software, which is based on the finite element method (FEM). This was performed by extracting and importing the SEM image of the fabricated CFPCF into COMSOL geometry interface. Convergence tests were executed by optimizing the mesh size and perfectly matched layer (PML) thickness, which led to more accurate results. We used the built-in circular PML with 10 μm thickness, which is added in the outer region of structure [33]. The meshing is divided into three regions, which are the PML layer, cladding region, and core region (including the first two air-hole rings), as shown in Fig. 3(c). The core region is the densest area compared to the PML and the cladding region, which leads to more accurate computational analysis. The maximum mesh element size of the core is 0.2 μm while the cladding and PML regions' mesh sizes are 0.8 μm and 1.6 μm, respectively. The full structure is meshed with 1,221,576 number of smallest elements.

A. Theoretical Analysis for Polarization Characteristics of CFPCF

The theoretical analysis of the dispersion relation of CFPCF is subjected to the material properties of silica and copper microwire. Consequently, this analysis was supported by using Eqs. (1) and (2). For silica, the dispersion relation was calculated by using the Sellmeier equation as represented in Eq. (1) [34]:

$$n(\lambda) = \sqrt{1 + \sum_{i=1}^{3} \frac{P_i \lambda^2}{\lambda^2 - Q_i}}, \tag{1}$$

where n is the refractive index of silica, and λ is the wavelength. The Sellmeier coefficients are as follows: $P_1 = 0.6961663$, $P_2 = -0.4079426$, $P_3 = -0.8974794$, $Q_1 = 4.67914826 \times 10^{-3}$ μm^2, $Q_2 = 1.3512063 \times 10^{-2}$ μm^2, and $Q_3 = 97.9340254$ μm^2.

In addition, Eq. (2) was used to analyze the dispersion relation for copper in terms of their dielectric constant. The dielectric constant of copper has been modeled using a Drude plus two critical points (D2CP) [35–37]:

$$\epsilon(\lambda) = \epsilon_\infty - \frac{1}{\lambda_p^2 (1/\lambda^2 + i/\gamma_p \gamma)} + \sum_{j=1}^{\infty} \frac{A_j}{\lambda_j} \left[\frac{e^{i\psi j}}{1/\lambda_j - 1/\lambda - i\gamma j} + \frac{e^{-i\psi j}}{1/\lambda_j + 1/\lambda + i\gamma j} \right], \tag{2}$$

where λ_p is the plasma wavelength, γ_p is the damping with the function of wavelengths, λ_j is the interband transition wavelength, γ_j is the transition broadenings with the function of wavelengths, and A_j is the dimensionless critical point amplitudes. The corresponding coefficient values of the D2CP equation for permittivity (ϵ) of the copper were set according to the experimental data from Johnson and Christy, as shown in Table 1 [31,35]. The polarization characteristics of the CFPCF was investigated by analyzing the modal analysis of the CFPCF. The effective refractive index of the CFPCF was calculated from the modal analysis. The confinement loss (C_L) of the structure can be determined by considering the imaginary part of the effective refractive index (Im[n_{eff}]) and is defined by Eq. (3) [38]:

$$C_{L(x,y)}[dB/\text{cm}] = 8.686 \times k_0 \times I_m[n_{\text{eff}}] \times 10^4, \tag{3}$$

where $k_0 = 2\pi/\lambda$ is the wave propagation number in the free space and the wavelength λ is in micrometers. The core-guided mode will eventually match with that of the SPP mode, which can result in resonance loss peak at a particular wavelength, known as the resonance wavelength.

Table 1. Fit Parameters for the D2CP Model of Permittivity for Copper (Cu)

Parameter (Unit)	Data from Johnson and Christy [31]
ϵ_∞	4.5761
λ_p (nm)	138.24
γ_p (nm)	12790.84
A_1	3.5710
ψ_1 (rad)	0.7204
λ_1 (nm)	225.22
γ_1 (nm)	409.90
A_2	0.6167
ψ_2 (rad)	1.3077
λ_2 (nm)	560.97
γ_2 (nm)	4331.1

3. EXPERIMENTAL SETUP

The experimental setup to measure the transmission spectrum of the CFPCF was exhibited in Fig. 4. A supercontinuum source (SuperK, NKT Photonics) was used as the input light source. Efficient light coupling was ensured by using a 20× objective lens. Controlled polarization of input light was achieved by employing a linear polarizer followed by a polarization-maintaining fiber. The output light from the CFPCF was split into two directions by using a polarization beam splitter. A perpendicularly directed light beam reached the charge-coupled device (CCD) (MicronViewer 7290A, Electrophysics) camera via a 40× objective lens and neutral-density (ND) filter while a parallel beam was directed to an optical spectrum analyzer (OSA). The ND filter before the CCD was used to control the intensity of light. We ensured an upward orientation of the CFPCF during all measurements by checking its mode image on the CCD camera and the transmission spectrum was recorded by using the OSA.

4. RESULTS AND DISCUSSION

The SEM image of the CFPCF and the mode image was taken from the CCD camera as depicted in Figs. 5(a) and 5(b). We ensured the correct orientation of the CFPCF throughout the measurement of the transmission spectrum.

The dispersion relation and the modal analysis for different orders of SPP modes and the core-guided mode of the CFPCF in x-polarization (horizontally polarized) and y-polarization (vertically polarized) are depicted in Fig. 6. The effective refractive index of the second-order SPP mode is much higher than the effective refractive index of the core-guided mode. As a result, the second-order SPP mode would match to the core-guided mode at a wavelength larger than 2 μm. As shown in Fig. 6(a), the phase-matching phenomenon occurred when the effective refractive index of the third-order SPP mode crossed the effective refractive index of the x- and y-polarizations core-guided mode at the wavelengths of 1790 and 1890 nm, respectively. During this phase-matching phenomenon, the resonance loss of x- and y-polarizations reached a maximum with 37.0 dB/cm at 1790 and 19.7 dB/cm at 1890 nm, respectively, as illustrated in Fig. 6(b). The electric field distributions of the respective guiding modes of x- and y-polarizations at the phase-matching phenomenon were portrayed in Figs. 6(c) and 6(d). In addition, transverse electric field vector distribution of the x-polarization coupling of the core-guided and SPP modes shows that the lobe fields of the SPP mode are strongly attracted to core-guided lobe fields, as shown Fig. 7(a). In contrast, Fig. 7(b) exhibits the loss in the lobe fields of SPP modes toward y-polarization core-guided lobe fields. This is because of the metal position dependency where the position of the copper wire was horizontally placed next to the CFPCF's core. These indicate higher resonance loss for the x-polarized mode than y-polarized. The same observation was also reported elsewhere [29,35].

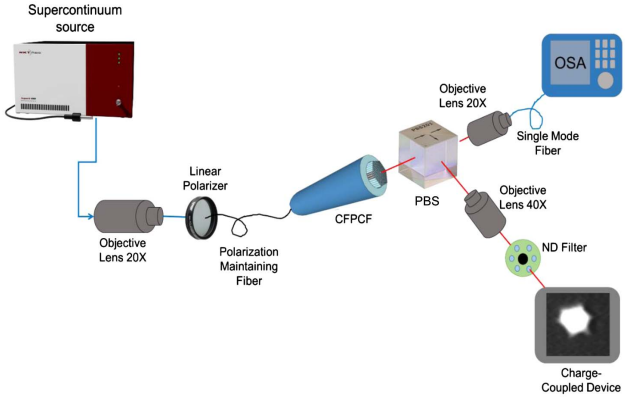

Fig. 4. Experimental setup for measuring the transmission spectrum.

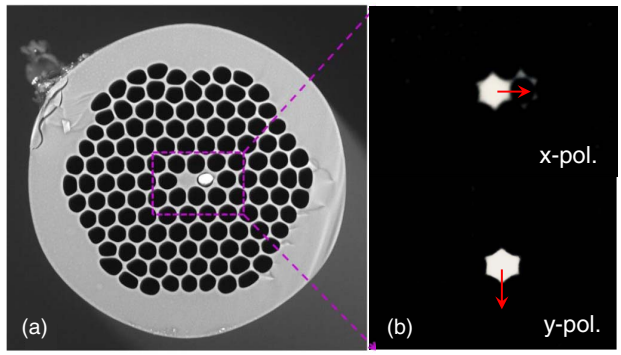

Fig. 5. (a) SEM image of the fabricated CFPCF, and (b) mode profile image taken from the CCD for x- and y-polarized modes.

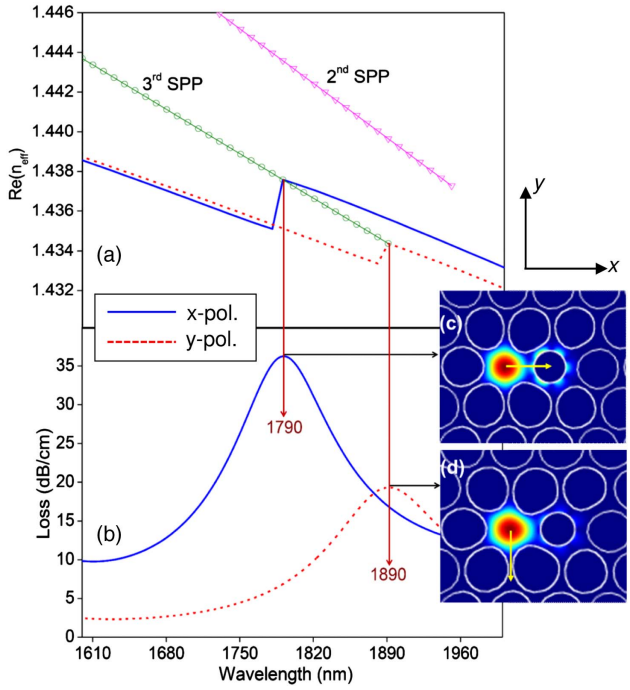

Fig. 6. Simulated results for (a) dispersion relation of the CFPCF polarization filter, (b) loss spectrum for the CFPCF for x- and y-polarizations. Electric field distribution of the fundamental mode of (c) x-polarization at 1790 nm and (d) y-polarization at 1890 nm.

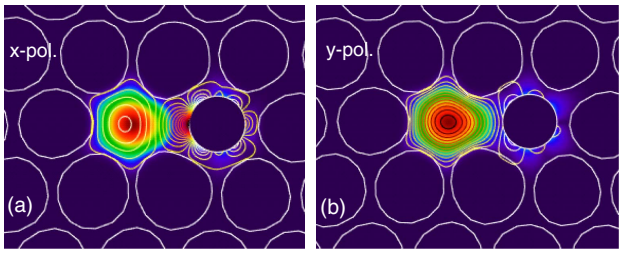

Fig. 7. Contour line of transverse electric field vector distribution of the (a) *x*-polarization, (b) *y*-polarization, representing the coupling strength of the phase-matching phenomena.

Figure 8 highlights the transmission spectra of *x*- and *y*-polarizations measured via a broadband source by using the OSA. Both measured transmission spectra (continuous line in blue color) have a resonance dip which corresponds to the phase-matching condition between the core-guided mode and the third SPP mode at the respective wavelengths of 1805 and 1910 nm. On the other hand, the transmission spectra of FEM simulation of *x*- and *y*-polarizations were observed at 1790 and 1890 nm, respectively. It is found that both measurements of resonance dips are shifted from their FEM simulations by 15 and 20 nm to a longer wavelength. This can be explained due to the thermal shrinkage of the metal during the fabrication, which led to form air gaps between the copper and the glass [39].

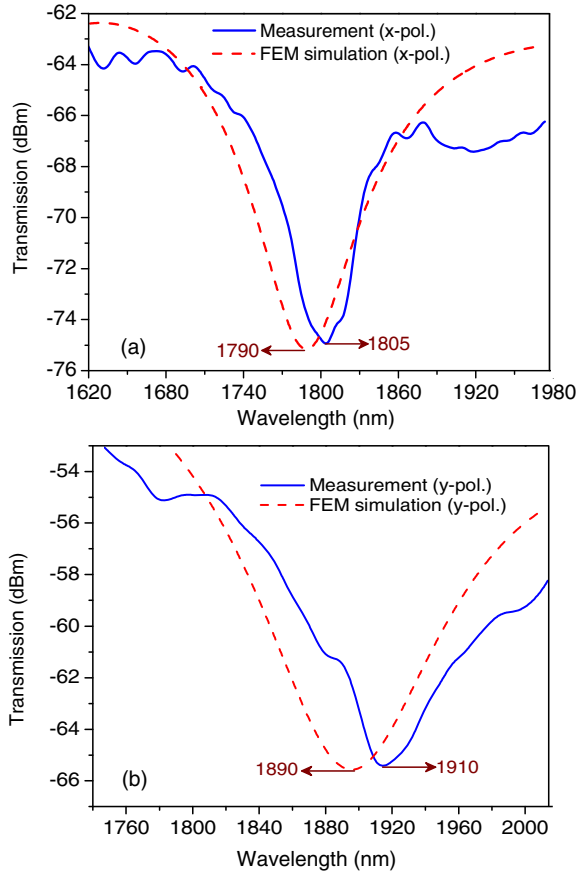

Fig. 8. Transmission spectra of measurement and FEM simulation: (a) *x*-polarization, (b) *y*-polarization.

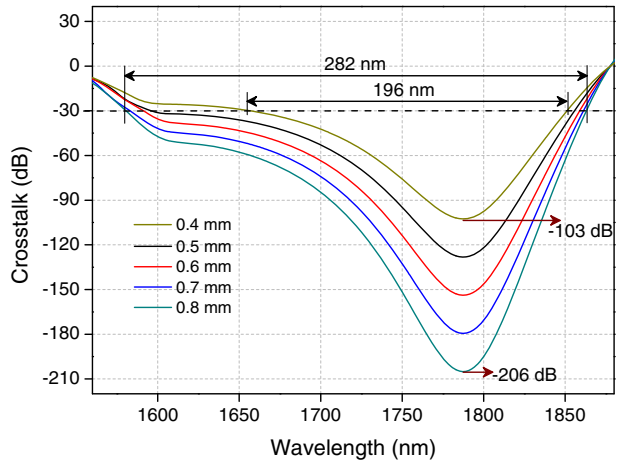

Fig. 9. Calculated cross talk for five different lengths of CFPCF polarization filter.

Cross talk is one of the key elements used to control and limit the undesirable polarized modes during the fabrication of a polarization filter. Cross talk also characterizes the quality

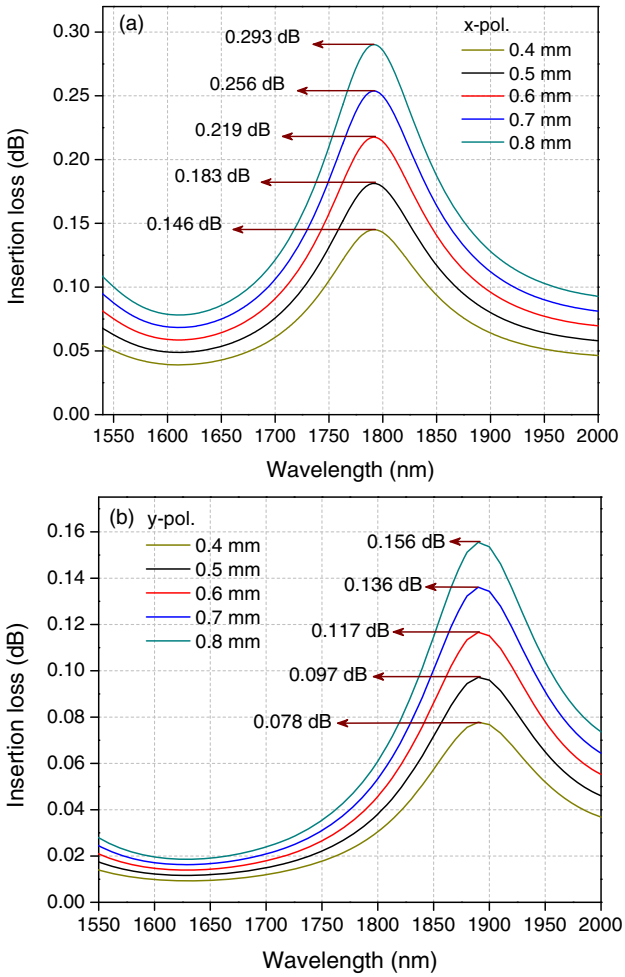

Fig. 10. IL with varying fiber length for (a) *x*-polarization, (b) *y*-polarization.

of transmission by defining its ability to eliminate the undesirable polarized mode [17]. The cross talk is developed by Beer–Lambert laws [29] in which it can be simplified as a function of the fiber length as given in Eq. (4):

$$\text{Crosstalk}[dB] = 20\log_{10}[\exp((C_{Lx} - C_{Ly})L)], \quad (4)$$

where L, C_{Lx}, and C_{Ly} are the length of the fiber and loss of x- and y-polarization modes, respectively. We have used the electromagnetic wave frequency domain for modal analysis based on the FEM to calculate cross talk which involves the imaginary part of the effective refractive index. Furthermore, the available optical bandwidth of the CFPCF can be measured as the wavelength encompasses within the cross-talk line below −30 dB [29].

Figure 9 presents the calculated cross talk of the CFPCF in different lengths as a function of wavelength. The cross-talk dip appears at the resonance wavelength of 1790 nm. As the fiber length increases, the degree of the cross talk increases too. The magnitude of cross talk for the shortest fiber length of 0.4 mm achieved is −103 dB, while the magnitude of cross talk reaches up to −206 dB for a 0.8 mm long CFPCF at the wavelength of 1790 nm. It is crucial for the cross talk to be sufficiently high as a polarization filter to eliminate the unwanted polarized mode and also retains a large optical bandwidth. The bandwidth of the 0.8 mm CFPCF is the widest, which is 282 nm (1580–1862 nm). Besides the confinement loss and the cross-talk value, the insertion loss (IL) is one of the key performances for the polarization filter. The IL can be calculated by considering the loss value of the wanted polarization mode. The IL of a filter can be calculated using Eq. (5) [40]:

$$IL_{x,y}[dB] = -10\log_{10}\left(\frac{P_{\text{out}(x,y)}}{P_{\text{in}(x,y)}}\right). \quad (5)$$

The ILs for both x- and y-polarizations by varying the fiber length are depicted in Fig. 10. As shown in Fig. 10(a), the IL for x-polarization has the highest peak at the resonance wavelength of 1790 nm with 0.8 mm fiber length, which gives 0.293 dB. Furthermore, at the y-polarized resonance wavelength (1890 nm), the IL of 0.156 dB is achieved with the 0.8 mm fiber length. It is noticeable that the IL for both x- and y-polarized modes is relatively low around 0.10 dB from the 1550 to 1700 nm wavelength. In general, the IL is increased when the length increased. These characteristics mentioned above would make the fabricated CFPCFs as the potential candidate for a polarization filter device.

A. Impact of Copper Wire Diameter on Characteristics of Polarization Filter

The characteristics of the polarization filter, such as the magnitude of the resonance loss, cross talk, and the optical

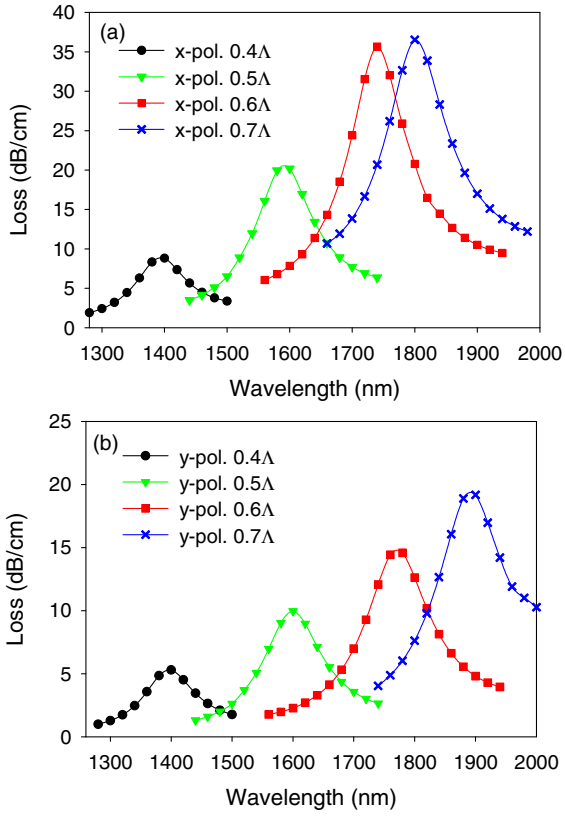

Fig. 11. Resonance loss of four different diameters of copper wire (d_c): (a) x-polarization and (b) y-polarization.

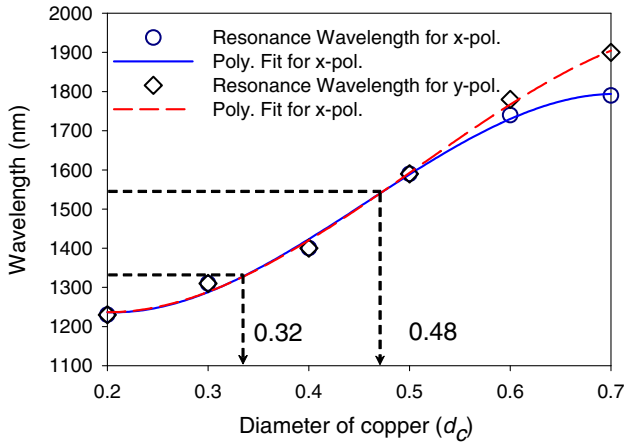

Fig. 12. Resonance wavelength for different diameters of copper wire.

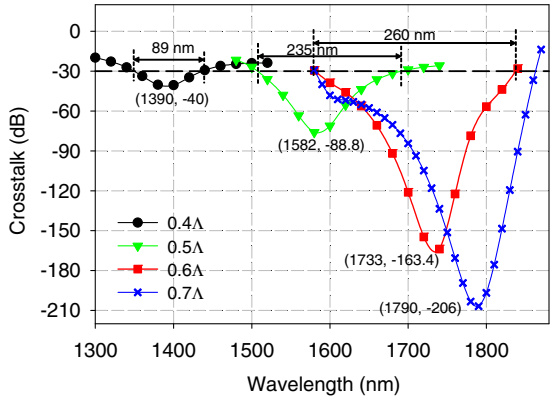

Fig. 13. Cross talk for 0.8 mm long CFPCF as a function of wavelength, considering different diameters of copper wire d_c.

Table 2. Polarization Characteristics with Respect to the Diameter of Copper Wire (d_c)

Diameter of Copper Wire, d_c (μm)	Resonance Loss in X-Polarized (dB/cm)	Resonance Loss in Y-Polarized (dB/cm)	Operating Wavelength X-Polarized (nm)	Operating Wavelength Y-Polarized (nm)	Cross Talk (dB)	Insertion Loss in X-Polarized (dB)	Insertion Loss in Y-Polarized (dB)	Bandwidth (nm)
0.4Λ	8.3	5.8	1390	1390	−40.0	0.071	0.042	89
0.5Λ	20.2	10.0	1582	1582	−88.8	0.016	0.080	235
0.6Λ	35.7	14.6	1733	1790	−163.4	0.286	0.117	260
0.7Λ	37.0	19.7	1790	1890	−206.0	0.293	0.156	282

bandwidth, can easily be altered by changing the diameter of the copper wire (d_c). Here, we considered phase matching of the third-order SPP mode with the core-guided mode to understand the impact of d_c on the polarization characteristics. The second-order's resonance coupling might be matched at the wavelength longer than 2000 nm. Four different d_c values of 0.4Λ, 0.5Λ, 0.6Λ, and 0.7Λ μm have been tested to understand the trend of resonance loss. As shown in Fig. 11, by increasing the d_c value, the magnitude of the resonance loss increases, while the resonance wavelength shifts toward the longer wavelengths. This trend is observed in both *x*- and *y*-polarizations, as depicted in Figs. 11(a) and 11(b), respectively. The results show by increasing the copper core diameter in the CFPCF from 0.4Λ, 0.5Λ, 0.6Λ, and 0.7Λ μm, the resonance losses of *x*-polarization are found to be 8.8, 20.2, 35.7, and 37 dB/cm, respectively. The corresponding resonance losses of *y*-polarization are observed to be 5.8, 11.2, 16.8, and 19.7 dB/cm. The dependency of the resonance wavelength to the diameter of the copper wire d_c is depicted in Fig. 12. The CFPCF can filter at communication wavelengths of 1310 and 1550 nm by choosing d_c to be 0.32Λ and 0.48Λ, respectively.

The amounts of cross talk for different d_c are shown in Fig. 13 for a fixed CFPCF length of 0.8 mm. The results show that the CFPCF with d_c of 0.4Λ, 0.5Λ, 0.6Λ, and 0.7Λ μm can filter the polarized light at the central wavelengths of 1390, 1582, 1733, and 1790 nm with cross-talk values of −40.0, −88.8, −163.4, and −206.0 dB and bandwidths of 89, 235, 260, and 282 nm, respectively, as summarized in Table 2.

5. CONCLUSION

In this study, we have designed and fabricated a simple structure of a polarization filter based on CFPCF. The CFPCF is fabricated by following the conventional stack-and-draw method. The resonance loss of the fabricated fiber is measured for *x*- and *y*-polarizations, which are 37.0 and 19.7 dB/cm, respectively. The measured transmission spectrum shows a good agreement with the simulated transmission of *x*- and *y*-polarizations with slight redshift in wavelength. Other characteristics of the CFPCF as polarization filter are numerically analyzed by using the SEM image of the fabricated fiber. The results show that the cross talk between *x*- and *y*-polarizations can be reduced by increasing the fiber length and/or the copper wire diameters. In the former approach, the central wavelength of the filter remains unchanged by increasing the fiber length, while in the latter method, the central wavelength shifts toward longer wavelengths as the copper diameter increases. For resonance loss and filter bandwidth, both of them are relatively increased by increasing the fiber length and/or copper diameter. It is shown that for a fixed length of 0.8 mm, by varying the diameter of the copper wire from 0.4Λ to 0.7Λ μm, the resonance wavelength can be tuned from 1390 to 1890 nm with a cross talk of −40 to −206 dB and bandwidth of 89 to 282 nm, respectively. Under the same circumstances, the insertion loss is relatively low for both polarizations. For *x*-polarization, the IL is ranging from 0.071 to 0.293 dB, whereas for *y*-polarization, the IL is ranging from 0.042 to 0.156 dB. Also, the CFPCF polarization filter can work in the communication bands of

1310 and 1550 nm by setting the copper diameter at 0.32Λ and 0.48Λ μm, respectively. The results suggest that the proposed CFPCF would be a suitable candidate for designing polarization filters. Furthermore, our CFPCF fabrication technique may open a new way to selectively fill the metallic wires inside microstructured fibers, which paves a broad range of applications.

REFERENCES

1. F.-J. Kao, Z.-Y. Chen, A. Gogoi, S.-Y. Lee, Y. Tsai-Lin, P.-W. Yi, M.-K. Lu, C.-C. Hsieh, J. Ren, and S. Marshall, "Coherent narrow-band light source for miniature endoscopes," IEEE J. Sel. Top. Quantum Electron. **25**, 1–10 (2018).
2. Y. Ye, L. Xiao, S. Dong, and A. C. Peacock, "Analysis of coupling losses for all-fiber integration of subwavelength core hybrid optical fibers," IEEE Photonics J. **10**, 1–12 (2018).
3. T. Yang, X. He, X. Zhou, Z. Lei, Y. Wang, J. Yang, D. Cai, S.-L. Chen, and X. Wang, "Surface plasmon cavities on optical fiber end-facets for biomolecule and ultrasound detection," Opt. Laser Technol. **101**, 468–478 (2018).
4. K. Wysokiński, D. Budnicki, J. Fidelus, Ł. Szostkiewicz, Ł. Ostrowski, M. Murawski, M. Staniszewski, M. Staniszewska, M. Napierała, and T. Nasiłowski, "Dual-core all-fiber integrated immunosensor for detection of protein antigens," Biosens. Bioelectron. **114**, 22–29 (2018).
5. C. Dou, X. Jing, S. Li, J. Wu, and Q. Wang, "A compact and low-loss polarization splitter based on dual-core photonic crystal fiber," Opt. Quantum Electron. **50**, 255 (2018).
6. A. A. Rifat, R. Ahmed, G. A. Mahdiraji, F. M. Adikan, and A. E. Miroshnichenko, "Highly sensitive selectively coated photonic crystal fiber-based plasmonic sensor," Opt. Lett. **43**, 891–894 (2018).
7. Z. Gong, R. Yin, W. Ji, J. Wang, C. Wu, X. Li, and S. Zhang, "Optimal design of dc-based polarization beam splitter in lithium niobate on insulator," Opt. Commun. **396**, 23–27 (2017).
8. L. H. Jiang, Y. Zheng, J. J. Yang, L. T. Hou, J. Y. Peng, and X. T. Zhao, "Design of an ultrashort single-polarization wavelength splitter based on gold-filled square-lattice photonic crystal fiber," Opt. Quantum Electron. **48**, 409 (2016).
9. M. F. O. Hameed, S. S. Obayya, and H. A. El-Mikati, "Highly nonlinear birefringent soft glass photonic crystal fiber with liquid crystal core," IEEE Photonics Technol. Lett. **23**, 1478–1480 (2011).
10. J. Ballato, T. Hawkins, P. Foy, B. Yazgan-Kokuoz, C. McMillen, L. Burka, S. Morris, R. Stolen, and R. Rice, "Advancements in semiconductor core optical fiber," Opt. Fiber Technol. **16**, 399–408 (2010).
11. J. C. Knight, "Photonic crystal fibres," Nature **424**, 847–851 (2003).
12. B. J. Eggleton, C. Kerbage, P. Westbrook, R. S. Windeler, and A. Hale, "Microstructured optical fiber devices," Opt. Express **9**, 698–713 (2001).
13. R. Bise, R. Windeler, K. Kranz, C. Kerbage, and B. Eggleton, "Tunable photonic band gap fiber," in *Optical Fiber Communication Conference* (Optical Society of America, 2002), p. ThK3.
14. C. Markos, K. Vlachos, and G. Kakarantzas, "Guiding and thermal properties of a hybrid polymer-infused photonic crystal fiber," Opt. Mater. Express **2**, 929–941 (2012).
15. J. Hou, D. Bird, A. George, S. Maier, B. T. Kuhlmey, and J. Knight, "Metallic mode confinement in microstructured fibres," Opt. Express **16**, 5983–5990 (2008).
16. J. Xue, S. Li, Y. Xiao, W. Qin, X. Xin, and X. Zhu, "Polarization filter characters of the gold-coated and the liquid filled photonic crystal fiber based on surface plasmon resonance," Opt. Express **21**, 13733–13740 (2013).
17. L. Chen, W. Zhang, Z. Zhang, Y. Liu, J. Sieg, L. Zhang, Q. Zhou, L. Wang, B. Wang, and T. Yan, "Design for a single-polarization photonic crystal fiber wavelength splitter based on hybrid-surface plasmon resonance," IEEE Photonics J. **6**, 1–9 (2014).
18. W. Zhang, S. G. Li, G. W. An, Z. K. Fan, and Y. J. Bao, "Polarization filter characteristics of photonic crystal fibers with square lattice and selectively filled gold wires," Appl. Opt. **53**, 2441–2445 (2014).
19. A. M. Heikal, F. F. K. Hussain, M. F. O. Hameed, and S. S. Obayya, "Efficient polarization filter design based on plasmonic photonic crystal fiber," J. Lightwave Technol. **33**, 2868–2875 (2015).
20. C. Dou, X. Jing, S. Li, Q. Liu, and J. Bian, "A photonic crystal fiber polarized filter at 1.55 μm based on surface plasmon resonance," Plasmonics **11**, 1163–1168 (2016).
21. P. Kumar, M. Senapati, and S. Das, "Designing photonic crystal fiber for optical sensor and medical application and suitable for wavelength division multiplexing systems," in *10th International Conference on Intelligent Systems and Control (ISCO)* (IEEE, 2016), pp. 1–4.
22. W. O. Carvalho, D. H. Spadoti, E. Silvestre, and F. Beltran-Mejia, "Ultralow chirp photonic crystal fiber Mach-Zehnder interferometer," Appl. Opt. **57**, 4228–4231 (2018).
23. R. Jorgenson and S. Yee, "A fiber-optic chemical sensor based on surface plasmon resonance," Sens. Actuators, B **12**, 213–220 (1993).
24. X. Zhang, R. Wang, F. Cox, B. Kuhlmey, and M. Large, "Selective coating of holes in microstructured optical fiber and its application to in-fiber absorptive polarizers," Opt. Express **15**, 16270–16278 (2007).
25. H. Tyagi, H. Lee, P. Uebel, M. Schmidt, N. Joly, M. Scharrer, and P. St. J. Russell, "Plasmon resonances on gold nanowires directly drawn in a step-index fiber," Opt. Lett. **35**, 2573–2575 (2010).
26. H. Lee, M. Schmidt, R. Russell, N. Joly, H. Tyagi, P. Uebel, and P. St. J. Russell, "Pressure-assisted melt-filling and optical characterization of Au nano-wires in microstructured fibers," Opt. Express **19**, 12180–12189 (2011).
27. P. Li and J. Zhao, "Polarization-dependent coupling in gold-filled dual-core photonic crystal fibers," Opt. Express **21**, 5232–5238 (2013).
28. H. Li, S. Li, H. Chen, J. Li, G. An, and J. Zi, "A polarization filter based on photonic crystal fiber with asymmetry around gold-coated holes," Plasmonics **11**, 103–108 (2016).
29. M. Li, L. Peng, G. Zhou, B. Li, Z. Hou, and C. Xia, "Design of photonic crystal fiber filter with narrow width and single-polarization based on surface plasmon resonance," IEEE Photonics J. **9**, 1–8 (2017).
30. M. Ordal, L. Long, R. Bell, S. Bell, R. Bell, R. Alexander, and C. Ward, "Optical properties of the metals Al, Co, Cu, Au, Fe, Pb, Ni, Pd, Pt, Ag, Ti, and W in the infrared and far infrared," Appl. Opt. **22**, 1099–1119 (1983).
31. P. B. Johnson and R.-W. Christy, "Optical constants of the noble metals," Phys. Rev. B **6**, 4370–4379 (1972).
32. G. Amouzad Mahdiraji, D. M. Chow, S. Sandoghchi, F. Amirkhan, E. Dermosesian, K. S. Yeo, Z. Kakaei, M. Ghomeishi, S. Y. Poh, S. Yu Gang, and F. R. Mahamd Adikan, "Challenges and solutions in fabrication of silica-based photonic crystal fibers: an experimental study," Fiber Integr. Opt. **33**, 85–104 (2014).
33. J.-P. Berenger, "A perfectly matched layer for the absorption of electromagnetic waves," J. Comput. Phys. **114**, 185–200 (1994).
34. B. Tatian, "Fitting refractive-index data with the Sellmeier dispersion formula," Appl. Opt. **23**, 4477–4485 (1984).
35. R. F. Ando, A. Tuniz, J. Kobelke, and M. A. Schmidt, "Analysis of nanogap-induced spectral blue-shifts of plasmons on fiber-integrated gold, silver and copper nanowires," Opt. Mater. Express **7**, 1486–1495 (2017).
36. H. Ehrenreich and H. Philipp, "Optical properties of Ag and Cu," Phys. Rev. **128**, 1622–1629 (1962).
37. P. G. Etchegoin, E. Le Ru, and M. Meyer, "An analytic model for the optical properties of gold," J. Chem. Phys. **125**, 164705 (2006).
38. A. Hochman and Y. Leviatan, "Calculation of confinement losses in photonic crystal fibers by use of a source-model technique," J. Opt. Soc. Am. B **22**, 474–480 (2005).
39. M. A. Schmidt, L. P. Sempere, H. K. Tyagi, C. G. Poulton, and P. St. J. Russell, "Waveguiding and plasmon resonances in two-dimensional photonic lattices of gold and silver nanowires," Phys. Rev. B **77**, 033417 (2008).
40. Y. Guo, J. Li, S. Li, S. Zhang, and Y. Liu, "Broadband single-polarization filter of d-shaped photonic crystal fiber with a micro-opening based on surface plasmon resonance," Appl. Opt. **57**, 8016–8022 (2018).